The dynamics of the Surface Treatment of Metals by Ultra-Short High-Power Laser Pulses

V. I. Mazhukin*, A. V. Mazhukin, M. M. Demin, A. V. Shapranov
Keldysh Institute of Applied Mathematics of RAS
Miusskaya sq. 4, Moscow, Russia.
*Email: vim@modhef.ru

Abstract

We consider the theory of fast phase transitions accompanying the ultrafast laser impact on metals. With the help of mathematical modeling defined the main regularities of surface modification of metal targets by picosecond and femtosecond laser pulses.

Surface Modification Technologies XXVI
Edited by T. S. Sudarshan, Micheal Jeandin and Vincent Firdirici

1.0. Introduction

The use of super-power $G \sim 10^{12}$–10^{15} W/cm^2 and ultra-short $\tau_L \approx 10^{-12}$–10^{-15} s laser pulses for dimensional processing of materials, such as cutting of various materials by pico-femtosecond laser pulses [1], micro-drilling by a femtosecond laser [2], surface etching of metals (Al, Cu, Mo, Ni) and semiconductors (Si) [3], is accompanied by realization of unique physical conditions. In particular, the duration of action becomes comparable with the characteristic times of thermalization and phase transitions in matter. This leads to the need to address complex fundamental problems, including the heating of the material and the kinetics of phase transitions in a strong deviation from local thermodynamic equilibrium.

It should be noted that the majority of laser technologies is associated with the beginning of phase transformations in the material. In particular, the action of pico - femtosecond laser pulses of high intensity on solid targets is one of the ways to create individual particles with unique characteristics, or to form their streams, consisting of a cluster, liquid or solid fragments of the target. The formation of the particle flux in the pulsed laser ablation is observed for a wide range of materials: metals, semiconductors and insulators.

Physics of supercooled states in metallic and nonmetallic systems, because of their widespread use in the production of new materials technology, is relatively well-studied[4]. Superheated states received little attention until recently, largely because of the difficulty of experimental investigation and non-obviousness of their application. The situation changed with the advent of femtosecond laser pulses and their application for the production of nanoparticles and nanomaterials [5, 6].

2.0. Mathematical description of processes in the irradiation zone

Laser radiation propagates from the right to the left and strikes the surface of the metal target. Then the radiation is partially absorbed and partially reflected. The absorbed energy is consumed for heating, phase transformations and the generation of shock waves in the solid phase. Fig. 1 shows spatial location of phases, moving interphase boundaries $r_{sl}(t)$, $r_{lv}(t)$ and shock wave in solid $r_{sh,s}(t)$.

Formulation of the problem was carried out under the following assumptions and limitations:

- The mechanisms of volume of melting and evaporation are not included into the consideration.
- The overheated metastable states act sustainably during the consideration.

The mathematical description and modeling of pico- and femtosecond laser action on metal target in vacuum was performed within the framework of a two-temperature and spatially one-dimensional multi-front nonequilibrium hydrodynamic Stefan problem, written for the two phases - solid and liquid.

2.1. System of equations

Action of high-power laser pulses on metal targets initiate in them a number of interrelated processes with nonlinear behavior. The description of their behavior is performed using a system of hydrodynamic equations, two energy balance equations for electron and phonon subsystems, and the transport equation of the laser radiation. The system of equations can be written in the domain with two moving boundaries $\Gamma_{sl}(t)$, $\Gamma_{kv}(t)$

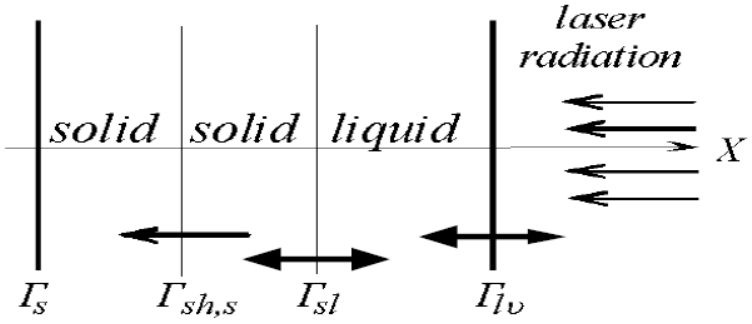

Fig. 1: Spatial phase configuration.

$$\left[\begin{array}{c} \frac{\partial\rho}{\partial t}+\frac{\partial(\rho u)}{\partial x} \\ \frac{\partial(\rho u)}{\partial t}+\frac{\partial(\rho u^2)}{\partial x}+\frac{\partial p}{\rho x}=0 \\ \frac{\partial(\rho_e\varepsilon_e)}{\partial t}+\frac{\partial(\rho_e u\varepsilon_e)}{\partial x}=-\left[p\frac{\partial u}{\partial x}+\frac{\partial W_e}{\partial x}+g(T_e)\left(T_e-T_{ph}\right)+\frac{\partial G}{\partial x}\right] \\ \frac{\partial\rho\varepsilon_{ph}}{\partial t}+\frac{\partial(\rho u\varepsilon_{ph})}{\partial x}=-\left[p\frac{\partial u}{\partial x}+\frac{\partial W_{ph}}{\partial x}-g(T_e)(T_e-T_{ph})\right] \\ \frac{\partial G}{\partial x}+\ \alpha(T_e)G=0,\ \rho_e=z\frac{m}{M}\rho, \\ P=P_e\left(\rho_e,T_e\right)+\ P_{ph}\left(\rho,T_p\right),\ \ \varepsilon_e=\ C_e(T_e)T_e,\ \varepsilon_{ph}=C_{ph}\left(T_{ph}\right)(T_{ph}) \end{array}\right]_{k=s,l} \quad \text{……..(1)}$$

$$t>0,\Gamma_s\ <x<\ \Gamma_{sh,s}(t)\cup\Gamma_{sh,s}\ (t)<x<\Gamma_{sl}(t)\cup\Gamma_{sl}(t)<x<\Gamma_{lv}(t),\ W_e$$
$$=\ -\lambda\left(T_e,T_{ph}\right)\frac{\partial T_e}{\partial x}\quad W_{ph}=\ -\lambda\left(T_{ph}\right)\frac{\partial T_{ph}}{\partial x},P(\rho,T)=P\left(\rho_eT_e\right)+P(\rho,T_{ph})$$

The designations: ρ*, u,* ε*, T, p* are the density, gas-dynamic velocity, internal energy, temperature and pressure correspondingly, $\alpha(T_e)$, $R(T_e)$ are the coefficient of volume absorption of the laser radiation and surface reflectivity, *G* is the density of the laser radiation, $C_e(T_e)$, $C_{ph}(T_{ph})$, $\alpha_e(T_e, T_{ph})$, $\alpha_{th}(T_{ph})$ are electron and phonon heat capacity and heat conductivity, *g(T) e* electron-phonon coupling factor. Indices *s*, *l,* υ, designate solid, liquid, vapor phases, *e, ph* designate electron and phonon components.

2.2. Initial conditions

$t=0,\ u(0,x)=0,\ p=0,\quad \rho=\rho_0,\ T_e=$
$T_p=T_0=293K$ .....(2)

2.3 Boundary conditions

On the left (fixed) boundary used condition of equal to zero mass and heat flow : $x=\Gamma_s$

$\rho_s u_s=0,\ W_T=0;$ ..... (3)

On the moving phase boundary $x=\Gamma_{sl}(t)$ used model of surface melting - crystallization represents a nonequilibrium kinetic variant of the Stefan problem [7–9], formulated for the conditions of strong deviations from local thermodynamic equilibrium.

$\rho_s(u_s - v_{sl}) = \rho_l(u_l - v_{sl}), P_s + \rho_s(u_s - v_{sl})^2 = P_l + \rho_l(u_l - v_{sl})^2, \left(\lambda_{ph}\frac{\partial T_{ph}}{\partial x}\right) - \left(\lambda_{ph}\frac{\partial T_{ph}}{\partial x}\right)_l = \rho_s L_m^{ne} v_{sl}$,.....(4)

These conservation laws are accompanied by the kinetic dependence of the interphase front velocity υ_{sl} (ΔT_{sl}) on the overheating of the solid surface.

$$\upsilon_{sl}(T_{sl}) = \frac{af}{\lambda}\left(\frac{3k_B T_{sl}}{m}\right)^{1/2}\left[1 - exp\left[\frac{L_m}{k_B}\left[\frac{\Delta T}{T_{sl}}\right]\right]\right] \quad \text{.....(5)}$$

Additional account of hydrodynamic effects was carried out using the expressions for the curve of equilibrium melting $T_m(P_s)$, temperature dependence of the equilibrium latent melting heat $L_m^{eq}(T_m * P_s))$ and non-equilibrium latent melting heat

$$L_m^{ne}: \quad L_m^{ne} = L_m^{eq}\big(T_m(P_s)\big) + \Delta C_{psl}\Delta T_{sl} + \frac{\rho_s+\rho_l}{\rho_s-\rho_l}\frac{(u_s-u_l)^2}{2}, \quad T_m = T_m(P_s) = T_{m,0} + kP_s,$$

where $\Delta C_{psl} = (C_{pl} - C_{ps})$, $\Delta T_{sl} = (T_{sl} - T_m(P_s))$

The electron component is assumed continuous with respect to the electron density N_e and temperature T_e during transition through the phase front:

$$\left[\lambda_e\frac{\partial T_e}{\partial x}\right]_s = \left[\lambda_e\frac{\partial T_e}{\partial x}\right]_l \qquad T_{es} = T_{el} \quad \text{.....(6)}$$

The model of surface evaporation is used as boundary conditions at the moving interphase boundary $\Gamma_{kv}(t)$. The process of surface evaporation within the approximation of the Knudsen layer is described by three conservation laws and three additional parameters at the outer side of the Knudsen layer (temperature T_υ, density ρ_υ and velocity u_υ). In the general case, two of these parameters (usually T_υ and ρ_υ) are determined using certain approximation relations, while the third one (usually the Mach number $M = u/u_c$) is found from the solution of the gas-dynamic equations.

$x = \Gamma_{k\upsilon}(t)$: $\rho_k(u_k - \upsilon_{k\upsilon})$, $p_k + \rho_k(u_k - \upsilon_{k\upsilon})^2 = p_\upsilon + \rho_\upsilon(u_k - \upsilon_{k\upsilon})^2$

$$\left[\lambda_{ph}\frac{\partial T_{ph}}{\partial x}\right]_k - \left[\lambda_\upsilon\frac{\partial T_\upsilon}{\partial x}\right]_\upsilon = \rho_k(u_k - \upsilon_{kv})L_\upsilon^{ne},$$
$$\rho_v = \alpha_\rho(M)\rho_{sat}, \quad T_v = \alpha_\rho(M)T_{sur}, \text{ .....(7)}$$

$$\rho_{sat} = \frac{p_{sat}(T_{sur})}{RT_{sur}},$$

$$p_{sat}(T_{sur}) = p_b exp\left[\frac{L_v^{ne}}{RT_b}\left[\frac{\Delta T_{sur}}{T_{sur}}\right]\right],$$

$$L_\upsilon^{eq} = L_\upsilon^{eq}(T_{sur}) + C_{pv}(T_\upsilon - T_{sur}) + \frac{\rho_k + \rho_\upsilon}{\rho_k - \rho_\upsilon}\frac{(u_k - u_\upsilon)^2}{2}$$

The boundary conditions for the electron component and the laser radiation are written as:

$$-\lambda_e\frac{\partial T_e}{\partial x} = \sigma T_e^4,$$
$$G(t) = \big(1 - R_k(T_e)\big).G_0 exp\left[-\left[\frac{t}{\tau_L}\right]^2\right] \text{..... (8)}$$

σ is the Stefan-Boltzmann constant.

3.0. Numerical algorithm

Mathematical feature of Stefan problems is the lack of explicit expressions for the interconnected quantities at the interphase boundaries: temperature T_{sl}, T_{sur} and velocities of the phase fronts υ_{sl} and υ_{kv}. So the problem (1) – (8) will be nonlinear even for constant values of thermo-physical and optical properties. For low velocities of phase transformations (υ_{sl} , $\upsilon_{kv} << \upsilon_{sound}$), the processes behave in a quasi-equilibrium way, and their description can be performed within the framework of equilibrium models. For example, in the problem of melting-crystallization, a phenomenological condition of the temperature equity $T_{sl} = T_s = T_l = T_m$ is used instead of the kinetic condition (5), and the differential Stefan condition is completely omitted.

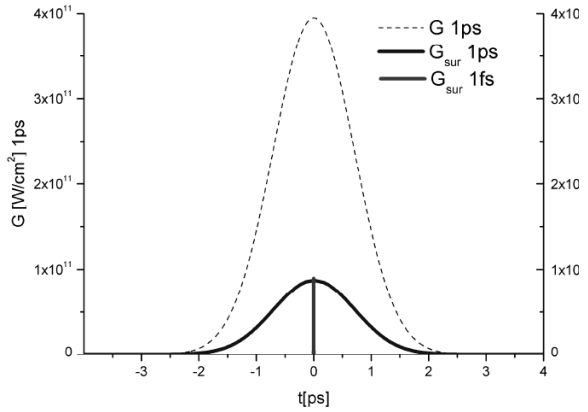

Fig. 2: Time profile of pico- and femtosecond pulses on the surface of Al.

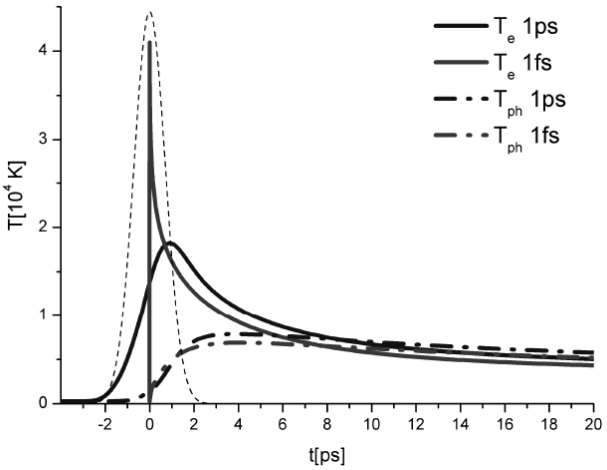

Fig. 3: Time dependence of the surface temperature of Al.

The influence of the phase transition is taken into account using a singular adding of the latent heat L_m^{eq} to the heat capacity (equation of state) in the point of the phase transition, so-called enthalpy method, in which the speed and location of the phase transition are determined implicitly.

Fast phase transitions ($\upsilon_{sl}, \upsilon_{kv} \ll \upsilon_{sound}$), that are typical for powerful pulsed laser action, occur under the conditions of high non-equilibrium caused by the powerful flow of material over the interphase boundary. High-speed phase transitions require explicit tracking of the phase boundaries [8]. Typically, the velocity of phase boundaries is determined numerically. In computational respect, the presence of moving boundaries leads to a significant complication of the numerical solution.

Finite-difference method of dynamic adaptation [9], was used to numerically solve the discussed problem. This method allows performing explicit tracking of any number of interphase boundaries and shock waves [10].

4.0. Modeling results

We consider two modes of pulse with pico - and femtosecond laser fluence with a wavelength $\lambda_l = 0.8\ \mu m$ on two metal target of aluminum (Al) and copper (Cu). The influence on each of the targets was carried out with the same energy density F, respectively $F = 0.7J\ cm^{-2}$ for Al and $F = 2.0\ J\ cm^{-2}$ for Cu. Fig. 2 shows the time profiles of the incident and the absorbed laser pulse with a Gaussian profile $\tau_L=10^{-12}$ s and $\tau_L= 10^{-13}$ s.

The incident laser radiation is absorbed in the electron component, causing it to warm up fast. The main feature of the nonequilibrium heating is that it occurs under conditions of intense competition between the rapid release of the laser energy and the factors limiting the heat - strongly varying electron thermal conductivity coefficient $\lambda_e(T_e,T_{ph})$ and electron-fonon coupling factor $g(T_e)$.

At picosecond influence $\tau_L=10^{-12}$, the maximum of electron temperature of the surface $T_{e,max} \approx 1.8\ x\ 10^4\ K$ is achieved at the descending branch of the laser pulse at the moment $t \cong \tau_L$, Fig. 3, and the values of the coefficients vary in the range $\lambda_{e,max}/\lambda_{Al}^{eq} \approx 10$ and $g_{max}/g_{Al}^{eq} \approx 70$. The maximum value of the lattice temperature is achieved after the pulse $t \approx 5\tau_L$ and amounts $T_{ph,\ max} \approx 7.5\ x\ 10^3\ K$. The maximum gap between the temperatures reaches the value, $\Delta T = T_e - T_{ph} \approx 10^4\ K$. Temperature equalization $T_e \approx T_{ph}$ occurs within a time ~ 10 ps.

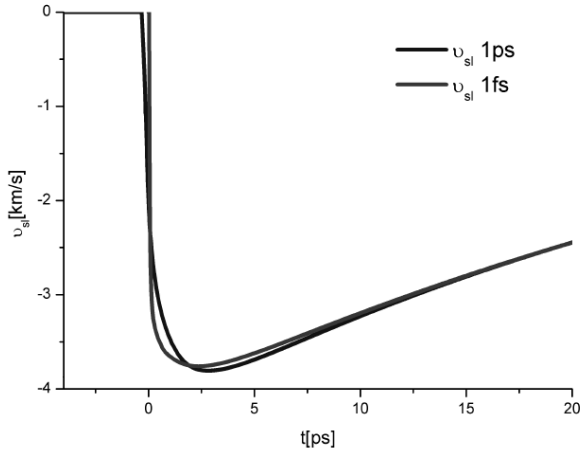

Fig. 4: The time profile of the velocity of melting of aluminum

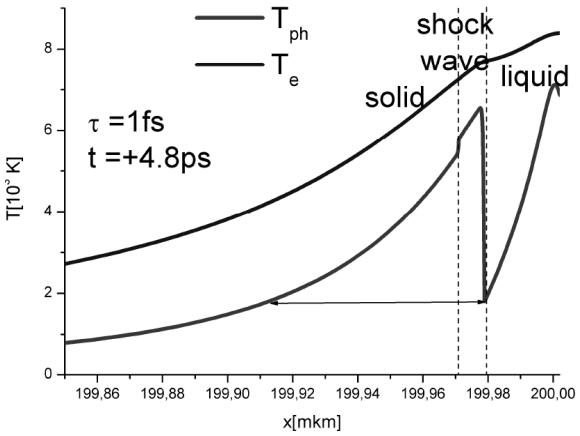

Fig. 5: The spatial profiles of temperature of aluminum.

Femtosecond influence $\tau_L=10^{-15}$ *s* differs from picosecond that the same energy is released during the 3 orders of magnitude less than that causes more of a deviation from local thermodynamic equilibrium. The values of the coefficients $\lambda_e(T_{em}\ T_{ph})$ and $g(T_e)$ limiting the heating of electronic components, and also increase $\lambda_{e,max}/\lambda_{Al}^{eq} \approx 27$ and $g_{max}/g_{Al}^{eq} \approx 200$, but not as much as *G(t)*. Time profile of the electron temperature of the surface $T_{e,surf}\,(t)$ significantly shifted relative to laser pulse time profile *G(t)* . The maximum value of the electron temperature is achieved at the end of the pulse $t \cong 2\tau_L$ and is $T_{e,max} \approx 4.1\ x\ 10^4\ K$, Fig. 3. A second difference of a femtosecond influence, despite the rapid energy exchange between the subsystems is a slow heating of the lattice, which differs little from the effects of heating at picosecond influence. The maximum value of the lattice temperature is achieved at the time $t \approx 5$ ps and is $T_{ph,max} \approx 7.2\ x\ 10^3$. The maximum gap between the temperatures reaches a value $\Delta T = T_e - T_{ph} \approx 3.3\ x10^4$ Temperature equalization $T_e \approx T_{ph}$ occurs within the time ~ 9 ps.

The high heating rate determines high rate of phase transformations. Fig. 4 shows the time dependences of the melting front propagation velocity $\upsilon_{sl}(t)$ for two modes of influence. Since the rate of heating of the lattice by pico – and femtosecond pulses differ slightly, then the rate υ_{sl} is almost the same. The only difference is in the initial stage of the process. At the picosecond influence, the birth of the melting front starts at the front of the laser pulse $t \approx -0.1$ *ps* , while at the femtosecond with a considerable delay after the pulse, $t \approx 30$ *fs* . The maximum values of $\upsilon_{sl,max}\,(t)$ = 3.75 km/s are achieved in the time interval $t \approx 2 \div 2.5$ *ps* . Such a high rate of propagation of the front leads to a pressure jump at the melting surface of the solid phase $p_s = 0.16$*Mbar* for $\tau_L=10^{-12}$*s* ($p_s = 0.14$ *Mbar* for $\tau_L = 10^{-15}$*s*) and the formation of a shock wave moving ahead of the front of melting, Fig. 5.

Appearance of high dynamic pressure causes an increase in the equilibrium melting temperature, the curve $T_m(p_s)$ shown in Fig. 6. Its maximum value reaches $T_m(p_s) \cong 1900$*K*. Due to the dynamic pressure of about one order of magnitude as compared to the equilibrium value, increases the value of non-equilibrium heat of melting $L_m^{ne}(p_s)$.

Comparison of the $T_{sl}(t)$ and $T_m(p_s(t))$curves indicates a significant overheating of surface of the phase boundary $T_{sl}(t) > T_m(p_s(t))$. The degree of nonequilibrium of melting process is conveniently characterized by the response function $\Delta t_{sl}(\upsilon_{sl})$, which is shown in Fig. 7.

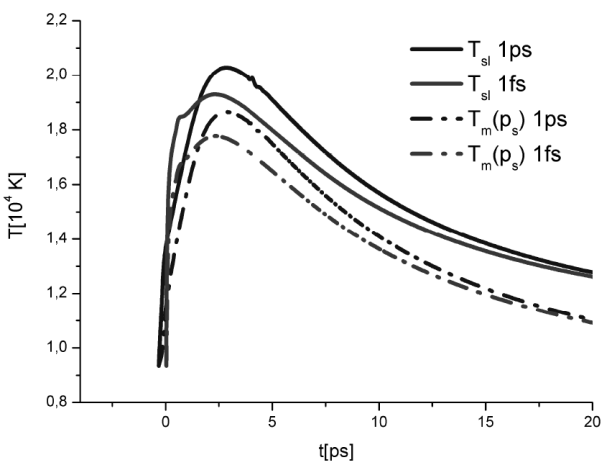

Fig. 6: The time profiles of the equilibrium melting temperature and temperature of the melting front of Al.

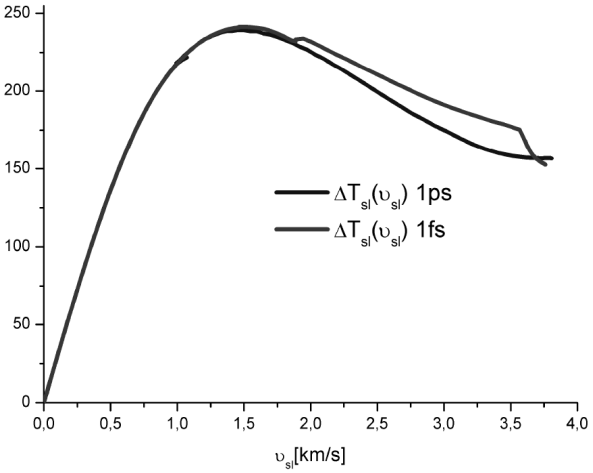

Fig. 7: Response functions $\Delta T_{sl}\,\upsilon_{sl}$ for Al.

At low overheating (supercooling), the function ΔT_{sl} increases linearly with growth υ_{sl}. In the range of υ_{sl} ~ 1 km/s, at which the shock wave is formed in the solid phase, ΔT_{sl} function has a smooth maximum indicating the change of the mechanism of phase transformation. The thermal conductivity mechanism is dominant at low velocities $\upsilon_{sl} \leq 1km/s$ will be displaced by hydrodynamic at large values $\upsilon_{sl} \leq \upsilon_{sound}$.

Fig. 8 shows fragment of dependence of υ_{sl} (t) which characterizes the hardening process which takes place in the nanosecond time range. Maximum velocity of the solidification front does not exceed 45 m/s, respectively, the maximum undercooling is $10 \div 15K$. High velocity of propagation of melting fronts are associated with strong cross-flows of matter and energy across the phase boundary.

In aggregate with volumetric nature of the energy transfer from the electron gas to the lattice it leads to the formation of highly superheated metastable state, characterized by the appearance of the surface temperature maximum $\Delta T_{ph,max} = T_{ph} - T_m(p_s) \approx 4.5 \cdot 10^3 K$ in the solid phase, Fig. 5. In the liquid phase is also formed near-surface temperature maximum, Fig. 8, but since the maximum velocity of evaporation front $\upsilon_{lv,max} \approx 40$ m/s is two orders of magnitude lower than the velocity υ_{sl} , magnitude and its role are insignificant.

Action of ultrashort laser pulses on metal target with different thermo-physical properties – copper – has several differences and many in common with the action of the aluminum target. The main difference of the non-equilibrium heating and non-equilibrium phase transformation in the condensed media is in the first place connected with the rate of energy exchange between the electron and phonon subsystems. The coefficient of energy exchange $g(T_e)$ in copper is by about 1.5 orders lower than that of aluminum, so that during laser energy release, the action of one of the main factors that limit the heating of the electron subsystem turns out to be significantly lower. As a result, the maximum values of the electron temperature of the surface are several times higher than that for aluminum $T_{e,max} \approx 4.\cdot 10^4 K$ for picosecond pulse $T_{e,max} \approx 1.2 \cdot 10^5 K$ for femtosecond pulse, Fig. 9.

Heating and melting of the lattice take place in the picosecond range $t_m \approx +0.1ps$, Fig. 10.

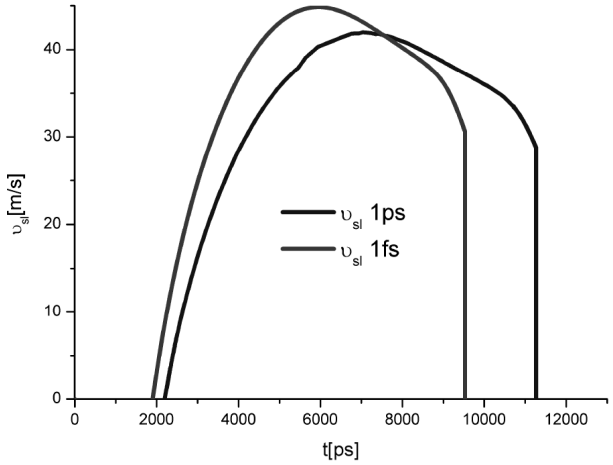

Fig. 8: The time profiles of the velocity of solidification of aluminum

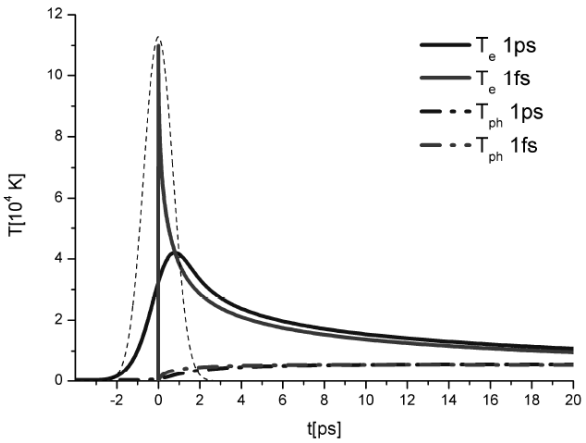

Fig. 9: Time dependence of the surface temperature of Cu.

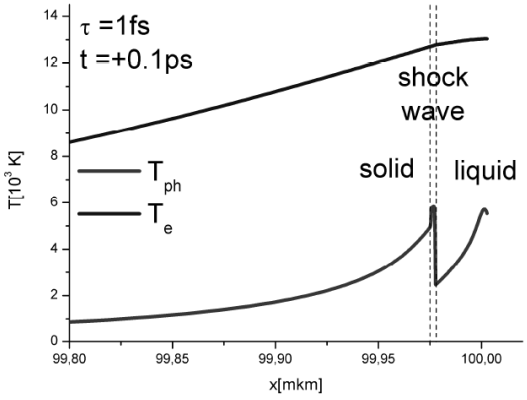

Fig. 10: The spatial profiles of temperature of copper.

For copper, the rate of energy transfer to the lattice is significantly lower, so that the velocity of the melting front turns out to be several times lower than that for aluminum $\upsilon_{sl,max} \approx 1.3\, km/s$, Fig. 11. The maximum value of the pressure in the solid phase is also lower $p_{s,max} \approx 0.14\, Mbar$. Despite the fact that the velocity υ_{sl} for copper is significantly lower than that for Al, the value of overheating of the interphase surface turns out to be significantly higher due to decrease of the hydrodynamic effects: $\Delta T_{sl,max} \approx 350K$, Fig. 12. The overheating of the sub-surface region of the solid phase reaches the value of $4.10^3 K$. The solidification of the liquid phase takes place in the nanosecond rage – the same as for aluminum. The lifetime of the melt reaches the value of $15 \div 10\, ns$, Fig. 13, the maximum velocity of the crystallization front - $\upsilon_{sl} \approx 35 m/s$. The maximum value of the overcooling of the front ~ *22 K*. The overcooling of the volume of the solid reaches the value of *800 K*. Modern experimental methods of the investigation of the processes of melting- crystallization of the metal systems determine the velocities of the solid-melt front to be within the range of 10–100m/s with corresponding overcooling of liquid within the range of $10 \div 400K$.

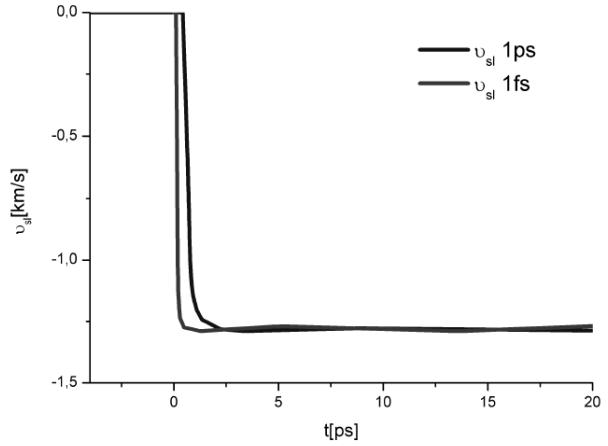

Fig. 11: The time profile of the velocity of melting of copper.

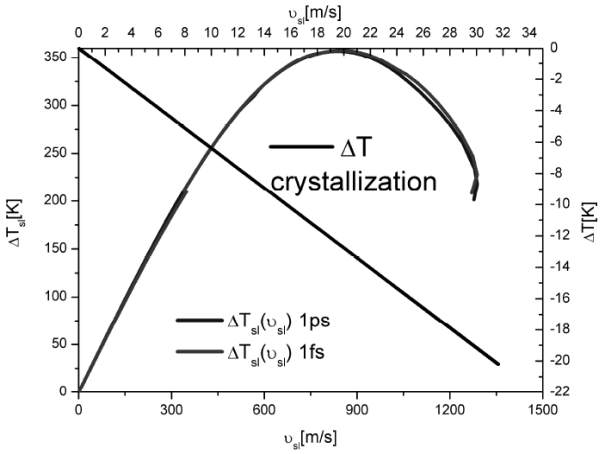

Fig. 12: Response functions $\Delta T_{sl}\,\upsilon_{sl}$ for Cu.

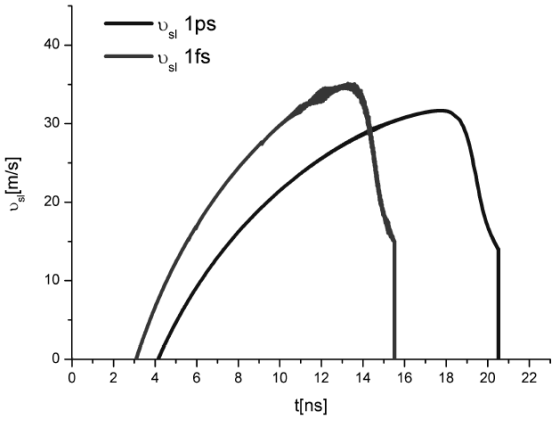

Fig. 13: The time profiles of the velocity of solidification of copper.

Thus, the data from the modeling of the metastable overcooled states in the liquid phase of metals is in relatively good agreement with the experimental measurements. It is not possible to perform the same comparison with the overcooled states in the solid phase because of the lack of reliable experimental data which is caused by the complexity of statement of such experiments.

5.0. Conclusion

The methods of mathematical modeling were used to investigate the regimes of pico- and femtosecond action on metals - Al, Cu. The kinetics and dynamics of phase transformations are analyzed. The results of the modeling confirmed the skewness of the high-speed processes of melting – solidification. In particular, the maximum velocity of melting reaches the value of several kilometers per second, while the maximum velocity of solidification does not exceed hundred of meters per second. The temperature dependence $\upsilon_{sl}(T_{sl})$ does not have a sharp bend in the point of change of the direction of the phase transition.

Special attention is paid to the overheated and overcooled metastable states that are caused by the fast phase transitions. The deviation from the local thermodynamical equilibrium is noticed both in the bulk and at the interphase boundary. The response function $T_{sl}(\upsilon_{sl})$ has a linearly increasing character for low values of velocity υ_{sl} in the range of $[0 \div \pm 50] m/s$. As the velocity υ_{sl} rises more than $\upsilon_{sl} > 100 m/s$, a maximum is formed in the response function for both metals. The appearance of the maximum means that the dominating mechanism of the phase transition changes: the mechanism of heat conductivity is changed by the hydrodynamic one. The maximum value of overheating of the interphase boundary reaches the value of $200 \div 400\ K$, the one for overcooling is by one order lower than that value. The overheating and overcooling of the bulk are significantly higher - $4 \cdot 10^3 \div 5 \cdot 10^3$ for overheating and $6 \cdot 10^2 \div 8 \cdot 10^2$ for overcooling. The results for different materials are compared between each other and with experimental data.

6.0. References

1. Ostendorf, A.; Kamlage, G.; Klug, U.; Korte, F.; Chichkov, B.N.; Proc. SPIE, 2005, vol. 5713, p.1.
2. Kamlage, G.; Bauer, T.; Ostendorf, A.; Chichkov, B.N.; Appl. Phys. A., Mater. Sci. Process., 2003, vol.77, p. 307.
3. Lopez, J.; Kling, R.; Torres, R.; Lidoiff, A.; Delaigue, M.; Ricaud, S.; Hönninger, C.; Mottay, E.; Proc. SPIE, 2012, vol. 8243, p. 824300.
4. Herlach, D.M.; Galenko, P.K.; Holland-Moriz, D.; Metastable Materials from Undercooled Metallic Melts, 2005, p. 485.
5. Mene´ndez-Manjo´n, A.; Barcikowski, S.; Shafeev, G.A.; Mazhukin, V.I.; Chichkov, B.N.; Laser and Particle Beams, 2010, vol. 28, p. 45.
6. Stratakis, E.; Barberoglou, M.; Fotakis, C.; Viau, G.; Garcia, C.; Shafeev, G.A.; Opt. Express, 2009, vol. 17, p. 12650.
7. Mazhukin, V.I.; Samarskii, A.A.; Review. Surveys on Mathematics for Industry, 1994, vol. 4, (2), p. 85.
8. Mazhukin, V.I.; Mazhukin, A.V.; Demin, M.M.; Shapranov, A.V.; Opticheskiy zhurnal, 2011, vol.78(8), p. 29.
9. Mazhukin, A.V.; Mazhukin, V.I.; Zhurnal Vychislitel'nojj Matematiki I Matematicheskojj Fiziki, 2007, vol. 47(11), p. 1911.
10. Mazhukin, A.V.; Mazhukin, V.I.; Computational Mathematics and Mathematical Physics, 2007, vol. 47(11), p. 1833.
11. Breslavsky, P.V.; Mazhukin, V.; Computational Mathematics and Mathematical Physics, 2007, vol. 48(11), p. 2102.